Nanowire Antenna Absorption Probed with Time-Reversed Fourier Microscopy

Grzegorz Grzela,[†] Ramón Paniagua-Domínguez,[‡] Tommy Barten,[†] Dick van Dam,[§] José A. Sánchez-Gil,[‡] and Jaime Gómez Rivas*[,†,§]

[†]FOM Institute for Atomic and Molecular Physics (AMOLF), c/o Philips Research, High-Tech Campus 4, 5656 AE Eindhoven, The Netherlands

[‡]Instituto de Estructura de la Materia (IEM-CSIC), Consejo Superior de Investigaciones Científicas, Serrano 121, E-28006 Madrid, Spain

[§]COBRA Research Institute, Eindhoven University of Technology, P.O. Box 513, 5600 MB Eindhoven, The Netherlands

Supporting Information

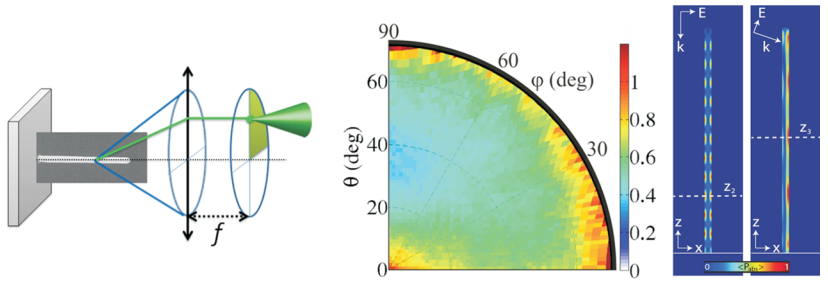

ABSTRACT: Understanding light absorption in individual nanostructures is crucial for optimizing the light-matter interaction at the nanoscale. Here, we introduce a technique named time-reversed Fourier microscopy that enables the measurement of the angle-dependent light absorption in dilute arrays of uncoupled semiconductor nanowires. Because of their large separation, the nanowires have a response that can be described in terms of individual nanostructures. The geometry of individual nanowires makes them behave as nanoantennas that show a strong interaction with the incident light. The angle-dependent absorption measurements, which are compared to numerical simulations and Mie scattering calculations, show the transition from guided-mode to Mie-resonance absorption in individual nanowires and the relative efficiency of these two absorption mechanisms in the same nanostructures. Mie theory fails to describe the absorption in finite-length vertical nanowires illuminated at small angles with respect to their axis. At these angles, the incident light is efficiently absorbed after being coupled to guided modes. Our findings are relevant for the design of nanowire-based photodetectors and solar cells with an optimum efficiency.

KEYWORDS: *Semiconductor Nanowires, Nanoantennas, Mie scattering, guided modes, absorption*

Semiconductor nanowires have attracted broad interest as building blocks for novel photodetectors and photovoltaic devices.[1−7] Similarly to other resonant nanostructures,[8−15] nanowires support optical modes to which the incident light can resonantly couple due to their small dimensions comparable to optical wavelengths. In this way, nanowires have proven to efficiently concentrate light and enhance absorption. Moreover, this absorption can be tuned by modifying the nanowire geometry making them act as nanoantennas for light.[16−20] Despite extensive theoretical and experimental investigations on light absorption in nanowire arrays and in solar cells,[17,21−28] the angle-dependent light absorption in individual nanowires remains largely unexplored.[29,30] Typically, only the two limiting cases for the illumination are reported in the literature: (i) nanowires lying on the substrate illuminated perpendicular to their axis that are described as Mie scatterers,[28,31−33] and (ii) vertical nanowires illuminated parallel to their axis that support guided modes to which the incident light can couple and be absorbed.[18,19,34]

Recently, the experimental comparison of the external quantum efficiency of vertical and horizontal single-nanowire solar cells has shown that nanowires exhibit a larger photocurrent when illuminated parallel to their axis.[35] However, this comparison was performed on different devices that did not contain the same nanowire and the intrinsic differences in the samples might have an impact on the results. To the best of our knowledge, the dependence of light absorption in uncoupled (individual) and the same nanowires on the angle of illumination has not been reported. These measurements are urgently needed as they will reveal the operational limits and the relative strength of the different absorption mechanisms. This knowledge is fundamentally interesting for understanding the interaction of light with these highly anisotropic structures

and crucial for improving the performance of nanowire-based solar cells and photodetectors.

In this manuscript, we demonstrate the angle-dependent light absorption in a dilute array of optically uncoupled nanowires that behave as individual nanowires, following a purely optical approach without using any electrical contacts to the wires. Such measurements rely on analyzing the light emission from nanowires and constitute an experimental challenge due to the very low intensity emitted to the far field by dilute nanowire arrays. We address this challenge by introducing a novel technique that we call time-reversed Fourier microscopy. With this technique, we are able to illuminate nanostructures under a microscope objective with a controlled and variable polarization and angle of incidence and efficiently collect their emission with the same objective. In this way, we can map the directional absorption of nanowires for the angles within the numerical aperture of the objective. We find that at small angles of incidence, measured from the nanowire axis, light predominantly couples to the HE_{11} guided mode, which is absorbed as it propagates through the wire. At large angles, however, the coupling to the guided mode weakens and the incident light excites Mie resonances that become the major absorption mechanism. The angle- and polarization-dependent absorption of the nanowires underlines their nanoantenna-like response to the incident light.

The manuscript is organized as follows: We first describe the sample consisting of an array of optically uncoupled InP nanowires. Second, we show dark-field microspectroscopy measurements on single nanowires and on small arrays of nanowires to find the signatures of Mie resonances on the scattered light by the nanowires. Next, we describe the time-reversed Fourier microscopy (TRFM) method used for the contactless measurements of angle-dependent light absorption in nanowires. These measurements are then explained using analytical and numerical modeling to find the relative contribution of the different absorption mechanisms present in nanowires.

Nanowire Description. The indium phosphide (InP) nanowires used in this work have been grown on top of a (111) InP substrate using the vapor−liquid−solid technique in a metal−organic vapor-phase epitaxy (MOVPE) reactor, as described in ref 36. The positions of the gold particle catalyzing the nanowire growth have been defined using electron beam lithography. To ensure that the light absorption in each nanowire is not affected by its neighbors, the distance between the gold catalyst particles is 5 μm, that is, much larger than the nanowire dimensions and the wavelength of light used in the experiment. The nanowires in this dilute array behave optically as individual nanostructures. As can be appreciated in the scanning electron microscope (SEM) image shown in Figure 1, the nanowires have an average diameter of $d = 100 \pm 10$ nm and a length of $L = 3.1 \pm 0.1$ μm.

Dark-Field Scattering Microscopy. We have investigated the dark-field scattering of individual vertical InP nanowires to characterize the excitation of Mie resonances. For these measurements, we have used dark-field confocal microspectroscopy. In our dark-field microscope, the nanowire is illuminated with white light from a halogen lamp in a range of elevation angles $\Delta\theta_i$ from 45 to 50°, regardless of the azimuthal incident angle φ_i. This illumination scheme is illustrated in Figure 2a. The scattered intensity at angles $\Delta\theta_s$ between 0 and ∼45° is collected by the objective and sent to a spectrometer (see Supporting Information for the details). The measured

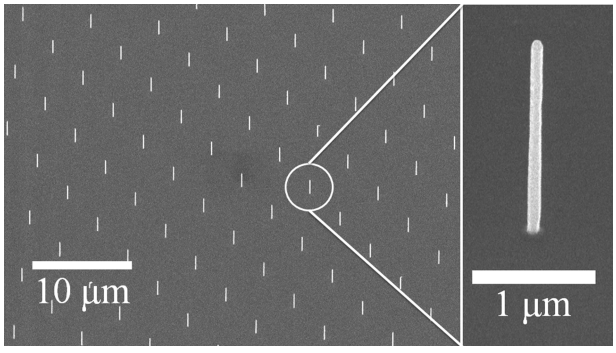

Figure 1. Scanning electron microscope image taken at an inclination of 30° of an InP nanowire array grown on top of an InP substrate. The array of nanowires has a pitch of 5 μm. Individual nanowires in this array have a length of 3.1 μm and diameters between 90 and 110 nm.

scattered intensity from a single nanowire is shown in Figure 2b. The spectrum, indicated by the black circles, shows one broad peak centered at $\lambda \sim 580$ nm. We compare this measured scattered intensity to the scattering efficiency of an infinitely long InP cylinder surrounded by air with a diameter of 110 nm calculated using Mie theory.[37] This calculation is represented by the red line in Figure 2b showing a good agreement with the measurements. It should be mentioned that this is the first time that the scattering spectra of vertical semiconductor nanowires have been compared to Mie theory, complementing the extensive work reported on horizontal nanowires.[28,31−33,38,39]

Scattering measurements of several InP nanowires have also been performed by expanding the field of view in the confocal microscope to illuminate an array of 6 × 6 nanowires. The result of these measurements is shown in Figure 2c with the black circles. The measured peak is broader than the peak obtained for a single wire, which can be attributed to the inhomogeneous broadening due to small variations in the nanowire diameter. The scattering efficiency, plotted with the red line in Figure 2c, is the averaged efficiency calculated using Mie theory for nanowire diameters between 90 and 110 nm. The good agreement between the measured scattered intensity and the calculated scattering efficiency demonstrates that the nanowires in the dilute array forming our sample behave as individual, or optically uncoupled scatterers.

Time-Reversed Fourier Microscopy for Angle-Dependent Absorptance Measurements. We have measured angle- and polarization-dependent light absorption of dilute arrays of nanowires using time-reversed Fourier microscopy. With this technique we create a collimated beam of light under a microscope objective by focusing a laser beam into a spot at the back focal plane (BFP) of the objective. This principle is illustrated in Figure 3a. The angle of incidence (θ_i, φ_i) on the sample, defined by the angle of the wave vector of the incident plane wave relative to the sample normal, depends on the location of the laser spot in the BFP. The position of this spot in the BFP is defined by scanning the laser mounted on a computer-controlled translation stage. Time-reversed Fourier microscopy corresponds to the reciprocal configuration of Fourier microscopy used to measure directional light emission and scattering.[36,40−48] Basic principles of Fourier microscopy are given in the Supporting Information. Time-reversed Fourier microscopy is conceptually similar to variable-angle epifluorescence microscopy (VAEM),[49] which is a variant of total internal reflection fluorescence microscopy.[50] In VAEM, a laser beam is focused in the BFP of an objective to make it incident

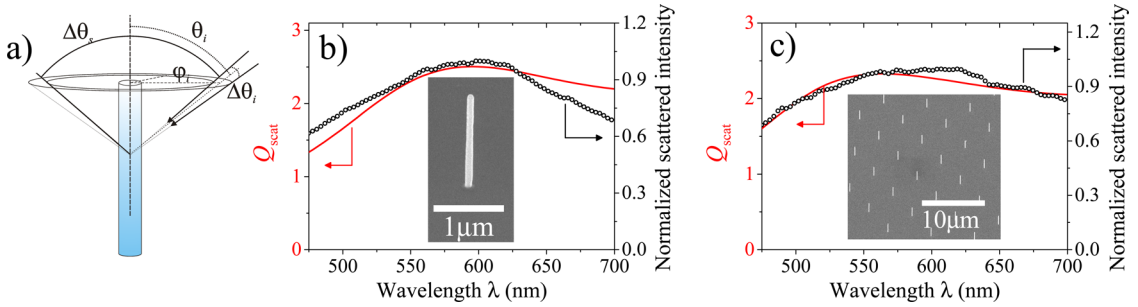

Figure 2. (a) Schematic representation for the dark-field scattering measurements. The light is incident along the ring defined by the range of elevation angles $\Delta\theta_i$. The scattered intensity in the cone with the apex angle $\Delta\theta_s$ is collected and detected. (b) Measured scattered spectrum of a single vertical InP nanowire (black circles). (c) Measured scattered spectrum from an array of 6 × 6 nanowires. The calculations of the scattering efficiency obtained from Mie theory are represented by the red lines. The scattering efficiency in (b) has been calculated for a single cylinder with a diameter of d = 110 nm. The scattering efficiency shown in (c) has been averaged over diameters between 90 and 110 nm with equal weights to account for the distribution of nanowire diameters in the sample.

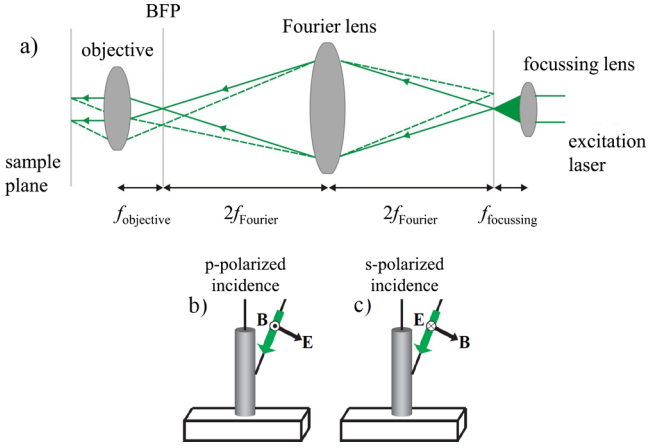

Figure 3. (a) Schematic representation of a Time-Reversed Fourier Microscope. A laser beam is focused to a spot at a particular position in the back focal plane of a microscope objective (BFP), effectively creating a quasi-point source in this plane. The light of the point source is transformed upon transmission by the objective into a collimated beam. The direction of the wave vector of this beam (that is, the angle of incidence on the sample) is determined by the position of the focused spot in the back focal plane. By varying this position we modify the angle of incidence of the beam onto the sample. In (b) and (c) the electric and magnetic fields orientations are shown for p- and s-polarization, respectively. The green arrow in the plots represents the incident wave vector.

onto a glass substrate at subcritical angles to control the depth of excitation of specimens for a more detailed imaging. In contrast, TRFM is not used to image the sample but to probe the angle-dependent light in absorption in nanostructures by the spectral analysis of the fluorescence. Figure 3b,c shows the orientation of the electric and the magnetic field vectors in the case of p- and s-polarized incident light. Pure p- or s-polarized excitation is achieved by scanning the position of the laser spot across the diameter of the BFP along the direction parallel or perpendicular to the polarization vector of the laser beam, respectively.

In the experiments, we have used a 100× microscope objective with a numerical aperture (NA) of 0.95. This NA allows angles of incidence θ_i up to about 70°. For the illumination, we have chosen a continuous-wave diode laser with a center wavelength of λ_0 = 532 nm. This wavelength is efficiently absorbed by InP. The power density of illumination was kept low ~4 W/cm^2 to avoid any nonlinear effects. Light absorption in individual nanowires was probed by measuring the intensity of the photoluminescence (PL) that was collected by the microscope objective. The nanowires were excited as a function of the angle of incidence (θ_i, φ_i) with a defined polarization. The excitation was filtered out using an edge-pass filter that transmitted wavelengths larger than 550 nm. Our setup collected the emission from approximately 16 uncoupled nanowires. The measured PL intensity $I_{NW}(\theta_i, \varphi_i)$ is proportional to the angle-dependent incident intensity $I_{in}(\theta_i, \varphi_i)$ times the angle-dependent absorptance of the nanowires $A_{NW}(\theta_i, \varphi_i)$

$$I_{NW}(\theta_i, \varphi_i) \propto I_{in}(\theta_i, \varphi_i) A_{NW}(\theta_i, \varphi_i) \tag{1}$$

The proportionality constant is independent of the angle of incidence but depends on the quantum yield of the nanowires and the angle-dependent emission of the nanowires integrated within the NA of the collection system. The quantum yield can vary significantly for different nanowires and is very difficult to obtain experimentally.[51] Also, the directionality of the emission might be nontrivial and depend strongly on the nanowire antenna dimensions.[36,52] Because $I_{in}(\theta_i, \varphi_i)$ depends only on the angle of incidence and is independent of the sample, we eliminate this contribution to the measurements by normalizing the $I_{NW}(\theta_i, \varphi_i)$ to the intensity emitted from a flat InP wafer upon the same illumination

$$\frac{I_{NW}(\theta_i, \varphi_i)}{I_{InP}(\theta_i, \varphi_i)} = C\frac{A_{NW}(\theta_i, \varphi_i)}{A_{InP}(\theta_i, \varphi_i)} \tag{2}$$

where $A_{InP}(\theta_i, \varphi_i)$ is the absorptance of the InP wafer and the constant C depends on the quantum yield of the emission of the nanowires and the InP wafer, as well as on the directionality of light emission from both structures integrated within the NA of the objective. From eq 2, we can write the angle-dependent light absorption of the nanowires as

$$A_{NW}(\theta_i, \varphi_i) = CA_{InP}(\theta_i, \varphi_i)\frac{I_{NW}(\theta_i, \varphi_i)}{I_{InP}(\theta_i, \varphi_i)} \equiv CF_{NW}(\theta_i, \varphi_i) \tag{3}$$

The term $A_{InP}(\theta_i, \varphi_i)$ can be calculated using the Fresnel coefficients for the air/InP interface knowing the permittivity of InP.[53] The product of this calculated absorption and the ratio of the measured PL intensities from the nanowires and the InP wafer gives the directional optical absorption in nanowires $F_{NW}(\theta_i, \varphi_i)$.

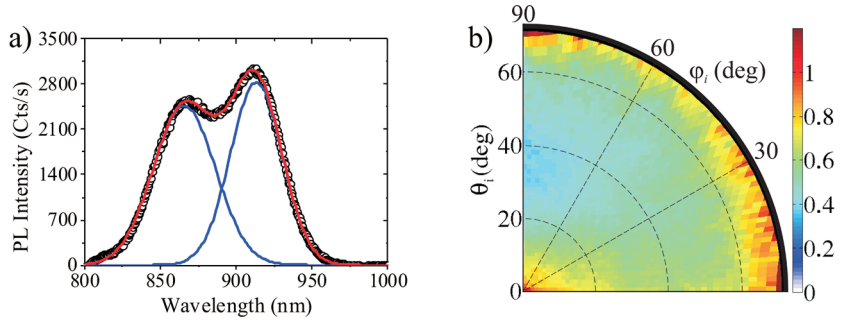

Figure 4. (a) PL spectrum of nanowires excited with light incident at $\theta_i = 0°$. The red solid line represents a double-Gaussian fit that is the sum of two individual Gaussians plotted with blue solid lines. (b) Normalized angle-dependent absorption pattern $F_{NW}(\theta_i, \varphi_i)$ of uncoupled nanowires obtained by scanning the position of the focused 532 nm laser spot in a quarter of the back focal plane of the microscope objective. The radius in this polar plot corresponds to the elevation angle of the incident beam θ_i, while the azimuthal angle corresponds to the azimuthal angle of incidence φ_i. The bottom horizontal edge ($\varphi_i = 0°$) of the absorption profile corresponds to p-polarized excitation, while the left vertical edge ($\varphi_i = 90°$) corresponds to s-polarized excitation. For other angles of incidence the polarization is a superposition of p- and s-polarized light.

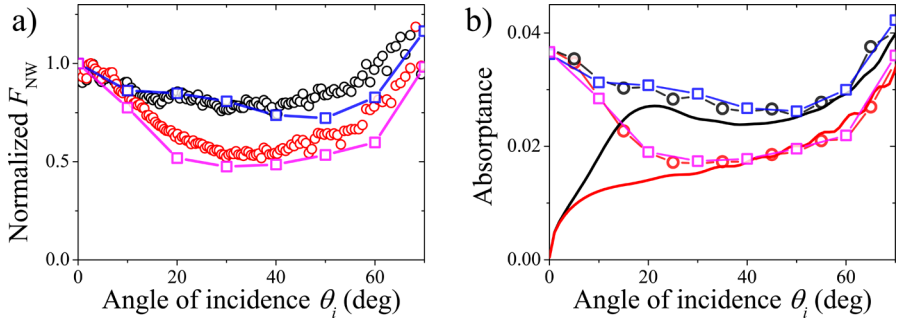

Figure 5. (a) Measured normalized directional absorption $F_{NW}(\varphi_i)$ of nanowires excited with p- and s-polarized light (black and red open circles, respectively) as a function of the angle of incidence. The blue and magenta open squares represent the simulated absorptance of the array of 100 nm-thick nanowires with a hexagonal cross section normalized to the value at $\theta_i = 0°$ (solid lines are guides to the eye). (b) The blue and magenta squares represent the same absorption as in (a), but plotted in the absolute values of absorptance. The black and red open circles are the simulated angle-dependent absorptance of an array of 90 nm-thick nanowires with a circular cross section for p- and s-polarized illumination, respectively. The solid lines connecting the symbols are guides to the eye. The solid lines in (b) show the absorptance of the effective medium consisting of 90 nm thick nanowires calculated using transfer matrix formalism. The black line corresponds to the p-polarized absorptance, while the red solid line plots the s-polarized absorptance.

The PL emission spectrum of nanowires upon excitation at $\theta_i = 0°$ is shown in Figure 4a. InP nanowires grow preferentially in the wurtzite crystal structure on top of the zincblende InP substrate.[54] Because the electronic band gap of InP in the wurtzite phase at room temperature is larger than that of zincblende, the emission peak of wurtzite nanowires is blue shifted compared to that of the substrate.[55,56] The maximum emission of the zincblende InP substrate is at $\lambda \sim 915$ nm while the maximum emission of nanowires is at $\lambda \sim 870$ nm. To differentiate the emission of the nanowires from the emission of the substrate, each spectrum has been fitted with a double-Gaussian function (red solid line in Figure 4a). The two constituting Gaussians of the fit are shown with the blue lines in this figure. A Gaussian fit is chosen because it represents the inhomogeneously broadened emission resulting from the local variations of the semiconductor band structure due to impurities and defects. The intensities of the nanowire emission as a function of the excitation angle and polarization have been extracted from the amplitude of the Gaussian peak centered at 870 nm. In this way, we only probe the angle-dependent absorption of the nanowires, discarding the contribution of the underlying substrate.

The directional absorption pattern $F_{NW}(\theta_i, \varphi_i)$ of a dilute array of uncoupled nanowires, normalized to its value at normal incidence, $\theta_i = 0°$, obtained by scanning one-quarter of the NA of the microscope objective is shown in Figure 4b. The bottom-left corner of this polar plot corresponds to the normal incidence, that is, the illumination parallel to the axis of nanowires. The radius measured from that corner corresponds to the elevation angle θ_i, while the azimuthal angle corresponds to angle φ_i measured from the horizontal edge of the plot. The absorption pattern is not cylindrically symmetric because the laser spot focused in the BFP was polarized along the direction $\varphi_i = 0°$. Such polarization resulted in a p-polarized illumination of the nanowires along $\varphi_i = 0°$ (bottom horizontal edge) and s-polarized excitation along $\varphi_i = 90°$ (left vertical edge of the pattern). In the other directions the polarization of excitation is a superposition of these two states. In the case of p-polarized excitation, the absorption pattern shows a high value at $\theta_i = 0°$ that decreases to a minimum at $\theta_i \sim 30°$ after which the absorption increases again. The absorption pattern for s-polarized excitation shows a maximum at $\theta_i = 0°$ and a more abrupt decrease than for p-polarized excitation until $\theta_i \sim 35°$. At larger angles, the s-polarized absorption increases again. An anisotropic absorption pattern with respect to the angle of incidence and polarization is characteristic for receiving nanoantennas.

Because of the nearly cylindrical symmetry of nanowires, $F_{NW}(\theta_i, \varphi_i)$ should not depend on φ_i as defined relative to the polarization axis, but it depends on θ_i and the polarization.

Therefore, we have performed more detailed line scans in the directions strictly corresponding to p- ($\varphi_i = 0°$) and s-polarized ($\varphi_i = 90°$) excitation in the range of θ_i from 0 to 70°. Figure 5a shows the directional light absorption in nanowire antennas $F_{NW}(\theta_i)$ for p- (black open circles) and s-polarized (red open circles) excitation, obtained from the time-reversed Fourier microscopy measurements and normalized to the value at θ_i = 0°. Both measurements show high absorption at $\theta_i = 0°$ and their angular behavior is consistent with Figure 4b. In the following section, these measurements are compared to finite element simulations.

Theoretical Modeling. We have used finite-difference time-domain (FDTD) simulations to reproduce the angle-dependent light absorption in uncoupled nanowires (the details of the model can be found in the Supporting Information). These simulations consider a box periodic in the *x*- and *y*-directions with a size of 5 × 5 × 3.4 μm^3 in the (*x*, *y*, *z*) directions, respectively. The simulation box consists of one InP nanowire with a hexagonal cross section with a diameter of 100 nm measured from the center of the hexagon to the vertex (circumradius) and a length of 3.1 μm. The nanowire stands vertical on top of an absorbing InP substrate. For both, the nanowire and the substrate, we used the refractive index of the zincblende InP, as the refractive index of wurtzite InP has never been determined experimentally. The periodic repetition of the simulation volume effectively results in considering a dilute two-dimensional array of uncoupled nanowires. To simulate the absorptance of the nanowires alone, we placed a power monitor only for the nanowires. The array is illuminated with a plane wave source with a wavelength of λ_0 = 532 nm at different angles of incidence and for p- and s-polarizations. From these simulations, we obtain the angle-dependent absorptance of the array of uncoupled nanowire antennas. The blue and magenta open squares (connected with guides to the eye) in Figure 5a show the simulated absorptance for p- and s-polarized incident light, respectively, normalized to the value at $\theta_i = 0°$. The simulated angle-dependent absorptance shows a good agreement with the measurements for the respective polarizations, which are plotted in the same figure with open circles. The non-normalized values of the simulated absorptance are plotted in Figure 5b with blue and magenta open squares (connected with guides to the eye) for p- and s-polarized excitation, respectively. Despite the ultralow filling fraction (0.03%), the array of uncoupled nanowires absorbs ~3.7% of the incident light at θ_i = 0°. This remarkable property makes nanowires very interesting nanostructures for applications in photovoltaics and for sensitive photodetection.

In order to compare the simulations to Mie theory, we have determined the diameter of a circular cylinder that absorbs the same amount of light as the hexagonal cylinder.[57] The simulated directional absorptance of a circular cylinder with a diameter of 90 nm is plotted in Figure 5b with open circles for p- (black) and s-polarized (red) excitation, respectively. To compare the simulated angle-dependent optical absorptance to the predictions of Mie theory, we use the transfer matrix formalism for a system consisting of three planar layers: a semi-infinite layer of air, an effective medium with a refractive index $\tilde{n} = n + i\kappa$ and a thickness *L* equal to the nanowire length, and a semi-infinite substrate.[58,59] Because the volume filling fraction of the nanowires in the layer is only 0.03%, we assume that the real component of the effective refractive index *n* of the nanowire layer is that of air.[17,59−61] The angle-dependent imaginary component $\kappa(\theta_i)$ of the effective refractive index of the nanowire layer accounts for the scattering and absorption of incident light by nanowires.[59] Because of the low volume filling fraction, $\kappa(\theta_i)$ can be calculated using the independent scattering approximation, which gives the relation[37]

$$\frac{4\pi\kappa(\theta_i)}{\lambda_0} = (Q_{abs}(\theta_i) + Q_{scat}(\theta_i))dL\frac{N}{V} \quad (4)$$

where $Q_{abs}(\theta_i)$ and $Q_{scat}(\theta_i)$ are the angle-dependent absorption and scattering efficiencies of individual nanowires, respectively, *d* is the diameter of nanowires, and *N* is the number of nanowires in a volume *V*. Unlike the commonly used Maxwell-Garnett effective medium theory, the independent scattering approximation accounts for the resonant response of nanowires as a function of the angle of incidence and polarization of the incident light. From eq 4, we obtain

$$\kappa(\theta_i) = \frac{(Q_{abs}(\theta_i) + Q_{scat}(\theta_i))dL\lambda_0}{4\pi V}N \quad (5)$$

In our sample, we have $N = 1$ per volume $V = La^2$, where *a* is the lattice constant of the nanowire array. Light scattered by the nanowires is not expected to contribute significantly to the absorption in their neighbors due to the large separation between them. Therefore, we assume that $Q_{scat}(\theta_i) = 0$ in eq 5 and that $\kappa(\theta_i)$ accounts only for the absorption of the incident light. The absorption efficiency for infinitely long nanowires can be calculated using Mie theory.[37] The underlying substrate is modeled using the real component of the refractive index of InP ($n = 3.7$), while the imaginary component is neglected in order to calculate the transmittance of the system. In this way, we can rule out the absorptance of the substrate from the calculations. Such approximation leads to a 1.6% relative decrease of the reflectance of the nonabsorbing InP substrate compared to the absorbing InP substrate. Because not all the reflected light by the substrate is absorbed by the nanowires, the error introduced by the approximation is even smaller than 1.6% and can be neglected. The absorptance of nanowires can be calculated assuming that $A(\theta_i) = 1 - T(\theta_i) - R(\theta_i)$, where $T(\theta_i)$ and $R(\theta_i)$ are the angle-dependent transmittance and reflectance of the multilayer system, respectively.

The black and red solid lines in Figure 5b show the absorptance calculated using the transfer matrix method based on the absorption efficiency of InP circular cylinders with a diameter of 90 nm obtained from Mie theory for λ_0 = 532 nm and p- (black solid curve) and s-polarized (red solid curve) incident light, respectively. This absorptance obtained decreases to 0 at $\theta_i = 0°$ for both polarizations. The comparison of the calculated Mie-based absorptance and the simulations from Figure 5b (that reproduce the measured directional absorption in Figure 5a) reveals that for small angles of incidence, up to $\theta_i \sim 30°$, Mie theory can not describe the angle-dependent absorption in the nanowires. For angles larger than $\theta_i \sim 30°$, the angular behaviors of the simulated and calculated absorptance show a good agreement for p-polarization with a local minimum at $\theta_i \sim 40°$ and increase for larger angles. The simulated and calculated s-polarized directional absorptance shows a good agreement for angles larger than $\theta_i \sim 30°$. At these angles, the s-polarized absorptance is visibly modulated by Fabry-Pérot resonances in the nanowire layer due to its finite thickness. The fact that the measurements, simulations, and calculations converge for both polarizations at large angles validates the independent scattering approximation made for the transfer matrix calculation and implies that the nanowires

behave as individual scatterers with an absorption at large angles of incidence dominated by light coupling to Mie resonances. It is worth pointing out that the absorptance of uncoupled nanowires at large angles can be larger than the absorptance at $\theta_i = 0°$ despite the lower absorption efficiency Q_{abs} (see Supporting Information). This happens due to the longer optical path in the nanowire layer and the reflection from the underlying substrate that supplies nanowires with more light to absorb. Such effect can be relevant when designing nanowire-based solar cells for harvesting direct and diffuse light.

While light coupling to Mie resonances seems to be the dominant process determining the absorptance for large angles of incidence, at small angles light couples to the nanowire from the top in a different way. To explain the origin of strong light absorption at $\theta_i = 0°$, we make use of rigorous numerical simulations (described in the Supporting Information). We consider a circularly cylindrical InP nanowire of diameter d = 90 nm and length L = 3.1 μm standing on top of a flat InP substrate. The simulations consider the complex refractive index of the InP nanowire and the real component of the refractive index of the InP substrate. The nature of the coupling of the normally incident light to the nanowire antennas can be explained by examining the near-field amplitudes in Figure 6. Figure 6a shows the amplitude of the total electric field in the x–z cross section illuminated at $\theta_i = 0°$ with a polarization vector along the x-direction. From the electric field variation along the nanowire, the light appears to couple to a guided mode. Such coupling has been previously observed in finite nanowires illuminated parallel to their axis or using focused excitation,[18,34] showing a strong dependence on the nanowire diameter.[20] It should be pointed out that the coupling of incident light to guided modes is forbidden for infinitely long cylinders due to the momentum mismatch between the wave vectors of light in free space and guided modes, therefore, this coupling is not considered in Mie theory.

The E_x component of the simulated electric field in the cross section of the nanowire (marked as the z_1 in Figure 6a), is plotted in Figure 6b. We compare this electric field component profile to the one of the HE_{11} guided mode supported by an infinitely long, 90 nm thick nonabsorbing cylinder with the same real component of the refractive index as in InP (n = 3.7) calculated analytically.[62] The respective analytically calculated E_x field profile is plotted in Figure 6c. The symmetry of the simulated field profile is in excellent agreement with the analytically calculated field profile of the HE_{11} guided mode, which confirms that the incident light couples to this guided mode in finite nanowires. The spatial map (absorption profile) of the time-averaged power absorbed per unit volume $\langle P_{abs} \rangle$ (see Supporting Information) in the x–z cross section of the nanowire illuminated at $\theta_i = 0°$ is shown in Figure 6d and resembles the symmetry of the HE_{11} guided mode. Figure 6e illustrates the simulated absorption profile $\langle P_{abs} \rangle_z$ of the E_z component of the electric field in the cross section of the nanowire (marked as z_2 in Figure 6d). This field component was chosen because of its characteristic pattern in the HE_{11} guided mode. We compare this simulated $\langle P_{abs} \rangle_z$ absorption profile to the analytically calculated one for the E_z component of the electric field in an infinitely long cylinder, which is plotted in Figure 6f. The agreement of the simulated and analytically calculated absorption profiles $\langle P_{abs} \rangle_z$ in the nanowire underlines the guided-mode character of the absorption in this nanostructure. Moreover, it is noticeable

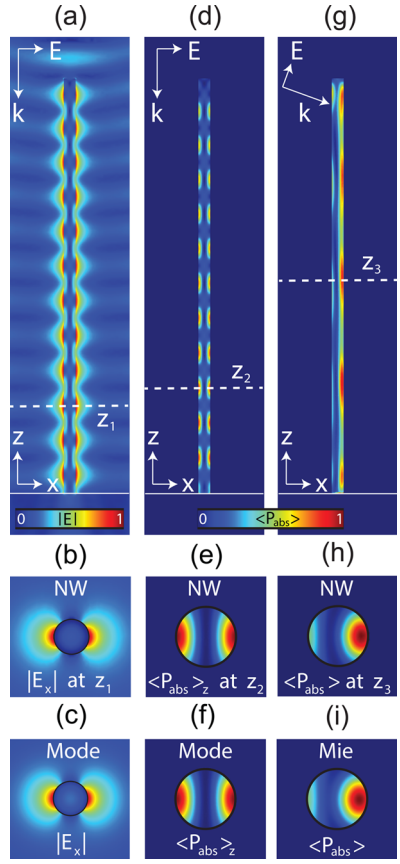

Figure 6. (a) Amplitude of the electric field around an InP nanowire standing on top of the InP substrate excited at $\theta_i = 0°$ with a plane wave with a wavelength of 532 nm and the polarization vector along the x-direction. The nanowire is 3.1 μm long and has a diameter of 90 nm. (b) Magnitude of the E_x component of the electric field in the horizontal cross section of the nanowire (marked as z_1 in panel a). (c) Magnitude of the E_x component of the electric field of the HE_{11} mode calculated analytically with a phase that corresponds to the z_1 position. (d) Spatial map of the time-averaged power absorbed per unit volume $\langle P_{abs} \rangle$ in the x–z cross-section of the same nanowire illuminated at $\theta_i = 0°$. (e) Simulated $\langle P_{abs} \rangle_z$ of the E_z component of the electric field in the horizontal cross section of the nanowire illuminated at $\theta_i = 0°$ (marked as z_2 in panel d). (f) Analytically calculated absorption profile $\langle P_{abs} \rangle_z$ of the E_z component of the electric field of the HE_{11} mode in the horizontal cross section of an infinitely long cylinder. The phase of the field is set to match the z_2 position in (d). (g) Spatial map of the time-averaged power absorbed per unit volume $\langle P_{abs} \rangle$ in the x–z cross-section of the same nanowire illuminated at $\theta_i = 70°$. (h) Simulated $\langle P_{abs} \rangle$ of the total electric field in the horizontal cross section of the nanowire illuminated at $\theta_i = 70°$ (marked as z_3 in panel g). (i) Analytically calculated absorption profile of the Mie resonance in the diameter of the corresponding infinitely long cylinder illuminated at $\theta_i = 70°$.

that the absorption is stronger in the bottom part of the nanowire even though light couples to the guided mode at the top facet and is gradually absorbed as the mode propagates in the nanowire. The increase of absorption in the bottom of the nanowire is related to the reflection of the guided mode at the bottom facet of the nanowire, reinforcing the absorption in the vicinity of this facet. The reflection occurs due to the difference between the effective refractive index of the guided mode (which in this case is close to 1) and that of the InP substrate (n = 3.7). This phenomenon depends on the confinement of the guided mode in the nanowire, which influences its

propagation length in the absorbing material. In thicker nanowires (e.g., 100 nm in diameter, simulation not shown here), the propagation length of the fundamental guided mode is shorter and the maximum absorption can occur in the top part of the nanowire.

We examine also the absorption profile in the nanowire illuminated at $\theta_i = 70°$, plotted in Figure 6g. This absorption profile is notably different from the one at $\theta_i = 0°$ incidence in Figure 6d and does not show the difference in the magnitude of the absorption between the top and the bottom of the wire. The white dashed line in Figure 6g indicates the $x-y$ cross section z_3 of the absorption profile in the diameter of the nanowire. This profile is displayed in Figure 6h and compared to the analytically calculated absorption profile in Mie resonance in an infinitely long cylinder of the same geometry, that is shown in Figure 6i. The similarities between the absorption profile in the finite nanowire and infinite cylinder indicate that at large angles of incidence light is predominantly absorbed by the excitation of Mie resonances.

From the theoretical analysis we conclude that light incident at small angles couples to the HE_{11} guided mode and propagates along the nanowire. This guided-mode is subsequently absorbed as it propagates, notably enhancing light absorption in individual InP nanowires at small angles of incidence with respect to their axis. For the investigated wavelength of illumination, the coupling of the incident light to guided modes outperforms the coupling to Mie resonances occurring at large angles of incidence. However, the absorptance of such an array at large angles of incidence can exceed the guided-mode absorptance at $\theta_i = 0°$ due to the longer optical path in the nanowire layer. Both types of coupling are not only angle-dependent but also diameter-, wavelength-, and length-dependent. The dimensions and orientation of nanowires used as solar cells should be carefully chosen so that the direct light couples to guided modes, while the diffuse sun light scattered by the atmosphere is harvested via Mie resonances.[31,59,63,64]

Conclusions. We have developed a technique called time-reversed Fourier microscopy to illuminate microscopic samples with well-defined angles of incidence. Using this technique we have measured the angle-dependent light absorption in dilute arrays of vertical InP nanowire antennas. Our measurements demonstrate experimentally the limitations of Mie theory to describe the light absorption in vertical nanowires at small angles of incidence measured from the nanowire axis. We have also compared the absorption measurements to numerical simulations for nanowires with a finite length. These simulations revealed that at normal incidence light efficiently couples to the HE_{11} guided mode. As the angle of incidence increases, the coupling to the HE_{11} guided mode becomes less favorable and the coupling to Mie resonances prevails. Our results are relevant for the design of nanowire-based solar cells, where understanding and optimizing the angle-dependent absorption is important to improve the performance of such devices.

■ ASSOCIATED CONTENT

Supporting Information

Supporting information shows the details of dark-field scattering measurements, principles of Fourier imaging microscopy, details on numerical simulations, and absorption efficiency of single finite and infinite nanowires. This material is available free of charge via the Internet at http://pubs.acs.org.

■ AUTHOR INFORMATION

Corresponding Author

*E-mail: rivas@amolf.nl.

Notes

The authors declare no competing financial interest.

■ ACKNOWLEDGMENTS

The authors are grateful to Tilman Zehender, Erik P. A. M. Bakkers, and Jos E. M. Haverkort for providing the samples used in the experiments. This work is part of the research program of the "Stichting voor Fundamenteel Onderzoek der Materie (FOM)", which is financially supported by the "Nederlandse organisatie voor Wetenschappelijk Onderzoek (NWO)" and is part of an industrial partnership program between Philips and FOM. The work of Ramón Paniagua-Domínguez and José A. Sánchez-Gil has been supported in part by the Spanish "Ministerio de Economía y Competitividad" (projects Consolider-Ingenio EMET CSD2008-00066 and NANOPLAS+ FIS2012-31070) and the "Comunidad de Madrid" (MICROSERES network P2009/TIC1476). Ramón Paniagua-Domínguez acknowledges support from CSIC through a JAE-Pre grant.

■ REFERENCES

(1) Tian, B.; Zheng, X.; Kempa, T. J.; Fang, Y.; Yu, N.; Yu, G.; Huang, J.; Lieber, C. M. *Nature* **2007**, *449*, 885−889.

(2) Tsakalakos, L.; Balch, J.; Fronheiser, J.; Korevaar, B. A.; Sulima, O.; Rand, J. *Appl. Phys. Lett.* **2007**, *91*, 233117.

(3) Kelzenberg, M. D.; Turner-Evans, D. B.; Kayes, B. M.; Michael, A.; Putnam, M. C.; Lewis, N. S.; Atwater, H. A. *Nano Lett.* **2008**, *8*, 710−714.

(4) Stelzner, T.; Pietsch, M.; Andrä, G.; Falk, F.; Ose, E.; Christiansen, S. *Nanotechnology* **2008**, *19*, 295203.

(5) Goto, H.; Nosaki, K.; Tomioka, K.; Hara, S.; Hiruma, K.; Motohisa, J.; Fukui, T. *Appl. Phys. Express* **2009**, *2*, 5004.

(6) Garnett, E.; Yang, P. *Nano Lett.* **2010**, *10*, 1082−1087.

(7) Wallentin, J.; Anttu, N.; Asoli, D.; Huffman, M.; Åberg, I.; Magnusson, M. H.; Siefer, G.; Fuss-Kailuweit, P.; Dimroth, F.; Witzigmann, B.; Xu, H. Q.; Samuelson, L.; Deppert, K.; Borgström, M. T. *Science* **2013**, *339*, 1057−1060.

(8) Ferry, V. E.; Sweatlock, L. A.; Pacifici, D.; Atwater, H. A. *Nano Lett.* **2008**, *8*, 4391−4397.

(9) Teperik, T. V.; De Abajo, F. G.; Borisov, A.; Abdelsalam, M.; Bartlett, P.; Sugawara, Y.; Baumberg, J. *Nat. Photonics* **2008**, *2*, 299−301.

(10) Atwater, H. A.; Polman, A. *Nat. Mater.* **2010**, *9*, 205−213.

(11) Zhu, J.; Yu, Z.; Fan, S.; Cui, Y. *Mater. Sci. Eng. R Rep.* **2010**, *70*, 330−340.

(12) Aydin, K.; Ferry, V. E.; Briggs, R. M.; Atwater, H. A. *Nat. Commun.* **2011**, *2*, 517.

(13) Spinelli, P.; Verschuuren, M.; Polman, A. *Nat. Commun.* **2012**, *3*, 692.

(14) van de Groep, J.; Spinelli, P.; Polman, A. *Nano Lett.* **2012**, *12*, 3138−3144.

(15) Zhou, L.; Yu, X.; Zhu, J. *Nano Lett.* **2014**, *14* (2), 1093−1098.

(16) Fan, Z.; Kapadia, R.; Leu, P. W.; Zhang, X.; Chueh, Y.-L.; Takei, K.; Yu, K.; Jamshidi, A.; Rathore, A. A.; Ruebusch, D. J. M. W.; Javey, A. *Nano Lett.* **2010**, *10*, 3823−3827.

(17) Diedenhofen, S. L.; Janssen, O. T. A.; Grzela, G.; Bakkers, E. P. A. M.; Gómez Rivas, J. *ACS Nano* **2011**, *5*, 2316−2323.

(18) Wu, P. M.; Anttu, N.; Xu, H. Q.; Samuelson, L.; Pistol, M.-E. *Nano Lett.* **2012**, *12*, 1990−1995.

(19) Anttu, N.; Namazi, K. L.; Wu, P. M.; Yang, P.; Xu, H.; Xu, H. Q.; Håkanson, U. *Nano Res.* **2012**, *5*, 863−874.

(20) Anttu, N. *Opt. Lett.* **2013**, *38*, 730−732.

(21) Kupec, J.; Witzigmann, B. *Opt. Express* **2009**, *17*, 10399−10410.

(22) Lin, C.; Povinelli, M. L. *Opt. Express* **2009**, *17*, 19371−19381.
(23) Giblin, J.; Protasenko, V.; Kuno, M. *ACS Nano* **2009**, *3*, 1979−1987.
(24) Giblin, J.; Syed, M.; Banning, M. T.; Kuno, M.; Hartland, G. *ACS Nano* **2010**, *4*, 358−364.
(25) Sturmberg, B. C.; Dossou, K. B.; Botten, L. C.; Asatryan, A. A.; Poulton, C. G.; de Sterke, C. M.; McPhedran, R. C. *Opt. Express* **2011**, *19*, A1067−A1081.
(26) Wang, B.; Leu, P. W. *Opt. Lett.* **2012**, *37*, 3756−3758.
(27) Hu, S.; Chi, C.-Y.; Fountaine, K. T.; Yao, M.; Atwater, H. A.; Dapkus, P. D.; Lewis, N. S.; Zhou, C. *Energy Environ. Sci.* **2013**, *6*, 1879−1890.
(28) Mann, S. A.; Garnett, E. C. *Nano Lett.* **2013**, *13*, 3173−3178.
(29) Anttu, N.; Xu, H. *Opt. Express* **2013**, *21*, A558−A575.
(30) Anttu, N.; Iqbal, A.; Heurlin, M.; Samuelson, L.; Borgström, M. T.; Pistol, M.-E.; Yartsev, A. *Opt. Lett.* **2013**, *38*, 1449−1451.
(31) Cao, L.; White, J. S.; Park, J. S.; Schuller, J. A.; Clemens, B. M.; Brongersma, M. L. *Nat. Mater.* **2009**, *8*, 643−647.
(32) Cao, L.; Fan, P.; Vasudev, A. P.; White, J. S.; Yu, Z.; Cai, W.; Schuller, J. A.; Fan, S.; Brongersma, M. L. *Nano Lett.* **2010**, *10*, 439−45.
(33) Brönstrup, G.; Jahr, N.; Leiterer, C.; Csáki, A.; Fritzsche, W.; Christiansen, S. *ACS Nano* **2010**, *4*, 7113−7122.
(34) Seo, K.; Wober, M.; Steinvurzel, P.; Schonbrun, E.; Dan, Y.; Ellenbogen, T.; Crozier, K. B. *Nano Lett.* **2011**, *11*, 1851−1856.
(35) Krogstrup, P.; Jorgensen, H. I.; Heiss, M.; Demichel, O.; Holm, J. V.; Aagesen, M.; Nygard, J.; Fontcuberta i Morral, A. *Nat. Photonics* **2013**, *7*, 306−310, DOI: 10.1038/nphoton.2013.32.
(36) Grzela, G.; Paniagua-Domínguez, R.; Barten, T.; Fontana, Y.; Sánchez-Gil, J. A.; Gómez Rivas, J. *Nano Lett.* **2012**, *12*, 5481−5486.
(37) Bohren, C. F.; Huffman, D. R. *Absorption and Scattering of Light by Small Particles*; Wiley: New York, 1983.
(38) Cao, L.; Fan, P.; Barnard, E. S.; Brown, A. M.; Brongersma, M. L. *Nano Lett.* **2010**, *10*, 2649−54.
(39) Brönstrup, G.; Leiterer, C.; Jahr, N.; Gutsche, C.; Lysov, A.; Regolin, I.; Prost, W.; Tegude, F.-J.; Fritzsche, W.; Christiansen, S. *Nanotechnology* **2011**, *22*, 385201.
(40) Yoshita, M.; Koyama, K.; Baba, M.; Akiyama, H. *J. Appl. Phys.* **2002**, *92*, 862−865.
(41) Gómez Rivas, J.; Vecchi, G.; Giannini, V. *New J. Phys.* **2008**, *10*, 105007.
(42) Grandidier, J.; Massenot, S.; Des Francs, G. C.; Bouhelier, A.; Weeber, J.-C.; Markey, L.; Dereux, A.; Renger, J.; González, M.; Quidant, R. *Phys. Rev. B* **2008**, *78*, 245419.
(43) Seršić, I.; Tuambilangana, C.; Koenderink, A. F. *New J. Phys.* **2011**, *13*, 083019.
(44) Shegai, T.; Miljkovic, V. D.; Bao, K.; Xu, H.; Nordlander, P.; Johansson, P.; Käll, M. *Nano Lett.* **2011**, *11*, 706.
(45) Fontana, Y.; Grzela, G.; Bakkers, E. P. A. M.; Gómez Rivas, J. *Phys. Rev. B* **2012**, *86*, 245303.
(46) Wagner, R.; Heerklotz, L.; Kortenbruck, N.; Cichos, F. *Appl. Phys. Lett.* **2012**, *101*, 081904−081904.
(47) Zhu, W.; Wang, D.; Crozier, K. B. *Nano Lett.* **2012**, *12*, 6235−6243.
(48) Curto, A. G.; Taminiau, T. H.; Volpe, G.; Kreuzer, M. P.; Quidant, R.; van Hulst, N. F. *Nat. Commun.* **2013**, *4*, 1750.
(49) Konopka, C. A.; Bednarek, S. Y. *Plant J.* **2008**, *53*, 186−196.
(50) Axelrod, D. *Traffic* **2001**, *2*, 764−774.
(51) Duan, X.; Huang, Y.; Cui, Y.; Wang, J.; Lieber, C. M. *Nature* **2001**, *409*, 66−69.
(52) Paniagua-Domínguez, R.; Grzela, G.; Rivas, J. G.; Sánchez-Gil, J. A. *Nanoscale* **2013**, *5*, 10582−10590.
(53) Hecht, E. *Optics*, 4th ed.; Addison Wesley: Reading, MA, 2002.
(54) Glas, F.; Harmand, J. C.; Patriarche, G. *Phys. Rev. Lett.* **2007**, *99*, 146101.
(55) Mattila, M.; Hakkarainen, T.; Lipsanen, H.; Jiang, H.; Kauppinen, E. I. *Nanotechnology* **2006**, *17*, 1580.
(56) Mishra, A.; Titova, L. V.; Hoang, T. B.; Jackson, H. E.; Smith, L. M.; Yarrison-Rice, J. M.; Kim, Y.; Joyce, H. J.; Gao, Q.; Tan, H. H.; Jagadish, C. *Appl. Phys. Lett.* **2007**, *91*, 263104.
(57) Henneghien, A.-L.; Gayral, B.; Désières, Y.; Gérard, J.-M. *J. Opt. Soc. Am. B* **2009**, *26*, 2396−2403.
(58) Yeh, P. *Optical waves in layered media*; Wiley: New York, 1988.
(59) Grzela, G.; Hourlier, D.; Rivas, J. G. *Phys. Rev. B* **2012**, *86*, 045305.
(60) Kirchner, A.; Busch, K.; Soukoulis, C. M. *Phys. Rev. B* **1998**, *57*, 277−288.
(61) Zhu, J.; Yu, Z.; Burkhard, G. F.; Hsu, C.-M.; Connor, S. T.; Xu, Y.; Wang, Q.; McGehee, M.; Fan, S.; Cui, Y. *Nano Lett.* **2009**, *9*, 279−282.
(62) Stratton, J. A. *Electromagnetic Theory. International Series in Pure and Applied Physics*; McGraw-Hill Book Company: New York, 1941.
(63) Muskens, O. L.; Gómez Rivas, J.; Algra, R. E.; Bakkers, E. P. A. M.; Lagendijk, A. *Nano Lett.* **2008**, *8*, 2638−2642.
(64) Brönstrup, G.; Garwe, F.; Csáki, A.; Fritzsche, W.; Steinbrück, A.; Christiansen, S. *Phys. Rev. B* **2011**, *84*, 125432.